Available online at www.sciencedirect.com
ScienceDirect
Journal of Power Sources 175 (2008) 60–67
JOURNAL OF POWER SOURCES
www.elsevier.com/locate/jpowsour

Thermodynamic predictions of the impact of fuel composition on the propensity of sulphur to interact with Ni and ceria-based anodes for solid oxide fuel cells

P. Lohsoontorn, D.J.L. Brett, N.P. Brandon *

Department of Earth Science and Engineering, Imperial College London, London SW7 2BP, United Kingdom

Received 30 April 2007; received in revised form 24 August 2007; accepted 23 September 2007
Available online 29 September 2007

Abstract

Thermodynamic calculations have been made to predict the stability of solid oxide fuel cell (SOFC) anode materials when exposed to hydrogen sulphide (H_2S) in hydrogen (H_2) over a range of partial pressures of sulphur (pS_2) and oxygen (pO_2) representative of fuel cell operating conditions. The study focussed on the behaviour of nickel and ceria, which form the basis of nickel–gadolinium-doped ceria (Ni-CGO) anodes, often used as an active layer within SOFCs. The reaction of Ni with sulphur is predicted to become more favourable as temperature and hydrogen partial pressure (pH_2) decrease. Ceria is shown to become increasingly non-stoichiometric (CeO_n, $n<2$) as pO_2 decreases and temperature increases, and it is predicted that its reaction with sulphur becomes more favourable under these conditions.

Keywords: Solid oxide fuel cell; Thermodynamics; Sulphur; Nickel; Ceria

1. Introduction

To extend the range of applications for solid oxide fuel cells (SOFCs), they should be as fuel flexible as possible. However, many fuels contain sulphur which, even at low (ppm) levels, may have a negative impact on SOFC performance. The quantity of sulphur contained in various fuel types ranges from a few ppm to over 1000 ppm. Several parts per million (ppm) of sulphur-containing impurity are added as an odorant to natural gas [1]. Commercial LPG contains 10–30 ppm sulphur depending on the supplier [2,3]. Sulphur contained in typical gasoline and diesel varies from 100 ppm to 500 ppm depending on the national regulations [4], while sulphur levels in biofuel can be over 1000 ppm. Sulphur is present in fuels in the form of many different compounds including thiophenes, mercaptans and organic sulphides [5]. However, sulphur compounds in a H_2-rich environment readily convert to H_2S under typical steam reformer or SOFC operating temperatures. Therefore, H_2S can be reasonably employed as the source of sulphur for assessing its impact on SOFC anodes.

This study uses thermodynamic calculations to explore the possible chemical interaction between Ni and ceria used in SOFC anodes with H_2S in H_2 concentrations found in operating devices. Results from these calculations are used to predict the propensity of the interaction of sulphur with Ni and ceria, when exposed to a sulphur-containing atmosphere in varied gas conditions (temperature, pH_2 and pH_2O).

1.1. Interaction of sulphur with nickel

Nickel (Ni) is widely used as the metallic component of anode cermets due to its good electrocatalytic activity, high electronic conductivity and relatively low cost. However, Ni (as a catalyst) is known to be poisoned by sulphur at concentrations of only a few ppm [5,6]. The interaction of sulphur compounds with Ni may involve a number of steps: adsorption and dissociation, reconstruction of the surface, formation of sulphide at the surface (two-dimensional surface sulphide) or in the bulk at higher sulphur concentration (three-dimensional metal sulphide) [7].

* Corresponding author. Tel.: +44 2075945704; fax: +44 2075947444.
E-mail address: n.brandon@imperial.ac.uk (N.P. Brandon).

0378-7753/$ – see front matter © 2007 Elsevier B.V. All rights reserved.
doi:10.1016/j.jpowsour.2007.09.065

The reaction of Ni with H_2S can be expressed as

$$1.5Ni + H_2S \leftrightarrow 0.5Ni_3S_2 + H_2 \quad (1)$$

Sulphur affects Ni activity in numerous ways. It degrades the catalytic activity of Ni through competitive adsorption with reactant species [7]. It can further react with Ni, forming sulphurous compounds on the surface leading to the blockage of active sites [8]. At a critically high sulphur coverage, nickel sulphides (e.g. Ni_3S_2) are formed as a bulk phase, decreasing the electronic conductivity compared to Ni (Ni_3S_2 has an electronic conductivity of approximately $10^2\ \Omega^{-1}\ cm^{-1}$ at room temperature [9]).

1.2. Interaction of sulphur with ceria

Doped ceria (notably with gadolinium) has been studied extensively and successfully applied as an anode cermet constituent for SOFCs operating at temperatures ranging from 773 K to 1173 K [10].

Ceria has also been studied as a potential desulphurization sorbent [11–13]. It is an important material for three-way catalysts and fluid catalyst cracking due to its redox behaviour and oxygen storage capacity.

As with other fluorite structured mixed valence oxides, ceria can deviate from stoichiometric cerium dioxide (CeO_2) to a non-stoichiometric form ($CeO_{2-x}, x<2$) [14]. With the ability to shift easily between reduced and oxidized states, it can release and uptake oxygen. Oxidation of reduced ceria occurs at room temperature while reduction starts from 473 K. Reduced-state ceria (CeO_{2-x}) is superior to CeO_2 in acting as an H_2S sorbent [15]. This suggests that reduced-state ceria is more likely to interact with sulphur than stoichiometric ceria in SOFC systems. The relevant reactions relating to ceria reacting with sulphur have been devised from sorbent development work [12,13]. CeO_2 can be reduced in the presence of H_2:

$$CeO_2 + xH_2 \leftrightarrow CeO_{2-x} + xH_2O \quad (2)$$

It can also be reduced when SO_2 is present:

$$CeO_2 + xSO_2 \rightarrow CeO_{2-x} + xSO_3 \quad (3)$$

Reduced-state ceria can react with H_2S forming a sulphide of ceria as shown by

$$2CeO_{2-x} + H_2S + (1-2x)H_2 \leftrightarrow Ce_2O_2S + (2-2x)H_2O \quad (4)$$

In the anode environment of an SOFC, the mixed ionic electronic conductivity (MIEC) of CGO has the beneficial effect of extending the triple phase boundary (TPB) away from the interface at which the electronically conducting phase, ionically conducting phase and continuous pore space combine, increasing the effective area over which the reactions necessary for fuel cell operation occur [15–17]. The formation of sulphur compounds on the metallic and ceramic components of the cermet can lead to the loss of active sites at the TPB and the modification of surface properties, so poisoning the anode [18]. It is also possible that the formation of a sulphide will affect the oxide transport and redox chemistry of ceria, affecting its MIEC properties and potentially reducing the effective TPB length.

2. Thermodynamic calculation procedure

The calculations were performed using HSC Chemistry® 5.1 [19] to generate phase diagrams of the ternary component systems of Ni–O–S and Ce–O–S. Cermets of nickel- and gadolinia-doped ceria (CGO) are being considered as an active layer to promote anode kinetics for solid oxide fuel cells operating over the temperature range 773–1173 K. Hence, the interaction between nickel, ceria and sulphur over this temperature range is of interest. The temperatures (673 K, 873 K, 1073 K and 1273 K) for phase diagrams were chosen to cover the ranges of ceria operation.

Gd was found to be far more resistant to reaction with sulphur than Ni and Ce, and due to its low (10 mol% in ceria) concentration in CGO, Gd was not considered further in this study. While a temperature at 873 K was taken as a reference point to represent the IT-SOFC temperature of operation frequently used with CGO electrolytes, temperatures of 673 K, 1073 K and 1273 K were also studied to explore the impact of temperature on sulphur interaction.

2.1. Bounds of practical fuel cell operation

In order to consider the area of interest in the phase diagram of Ni and ceria, the bounds of practical SOFC operation with respect to pS_2 and pO_2 at the anode need to be defined. The boundary values of pH_2 and pH_2O were calculated by assuming a mixture of 3% H_2O and 97% H_2 as the input to the anode, representing the extreme case of a hydrogen fuelled SOFC, and 90% H_2O and 10% H_2 as the output composition (representing 90% fuel consumption of a hydrogen fuelled SOFC). These capture the outer bounds of pO_2 that may be experienced within a SOFC device operating on reformed hydrocarbon fuels.

The pO_2 value was calculated using the correlation between the partial pressure of species and the equilibrium constant of the reaction:

$$2H_2 + O_2 \rightarrow 2H_2O \quad (5)$$

The bounds of pS_2 were defined to represent H_2S concentrations ranging between 1 ppm and 1000 ppm. The pO_2 value derived from Eq. (5) is used to calculate the value of pS_2. The pS_2 was calculated using the correlation between the partial pressure and the equilibrium constant of the two main reactions:

$$2H_2S + O_2 \rightarrow S_2 + 2H_2O \quad (6)$$

$$2H_2S \rightarrow 2H_2 + S_2 \quad (7)$$

The values of pO_2 and pS_2 for the various operating conditions, used to define the area of interest in Figs. 1, 2, 4 and 5, are presented in Table 1.

To study the impact of pH_2 on the propensity of the interaction of sulphur with Ni and ceria, a fuel composition of 20% H_2 (constant 3% H_2O) was chosen. However, this low amount

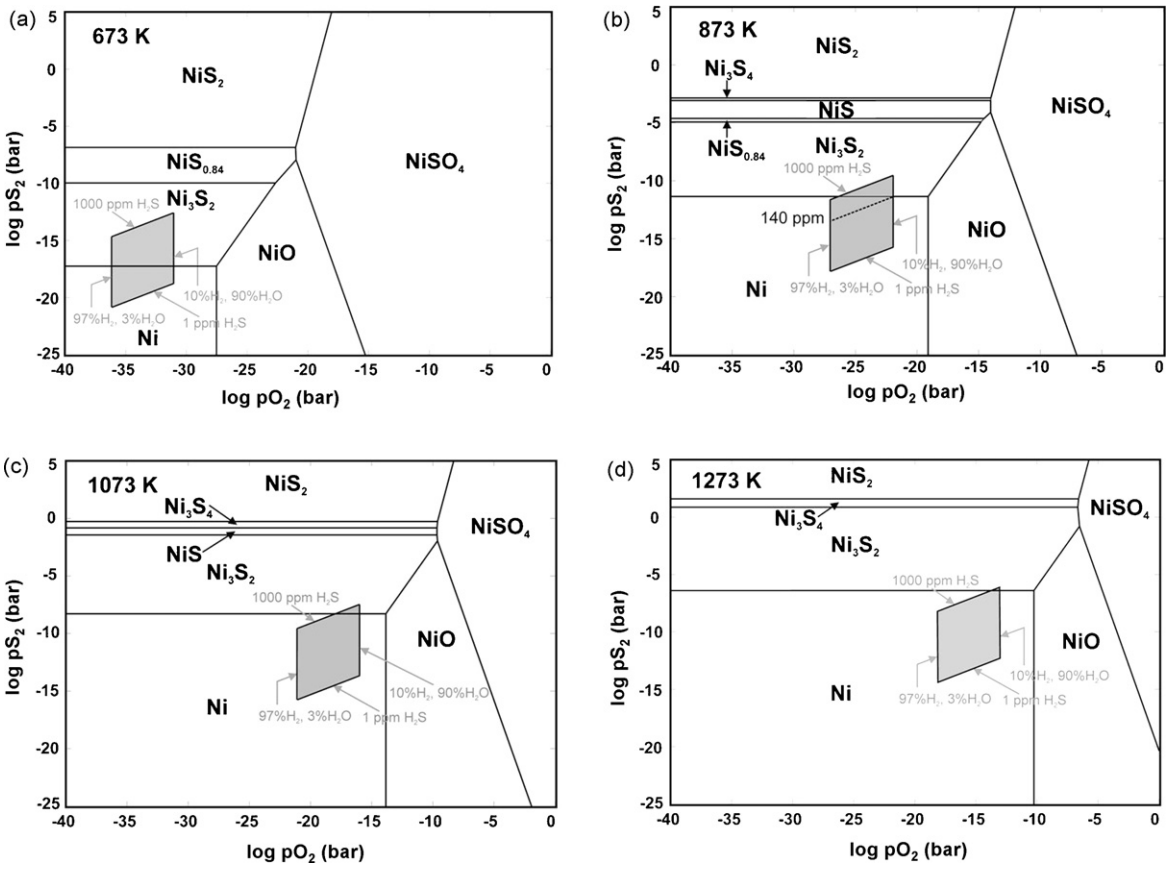

Fig. 1. (a) Phase equilibrium of the Ni–O–S system at 673 K. The shaded area shows the phases of Ni over an H_2S range of 1–1000 ppm in humidified hydrogen (97% H_2, 3% H_2O to 10% H_2, 90% H_2O). (b) Phase equilibrium of the Ni–O–S system at 873 K. The shaded area shows the phases of Ni over an H_2S range of 1–1000 ppm in humidified hydrogen (97% H_2, 3% H_2O to 10% H_2, 90% H_2O). The dotted line in the shaded area shows an H_2S concentration of 140 ppm. (c) Phase equilibrium of the Ni–O–S system at 1073 K. The shaded area shows the phases of Ni over an H_2S range of 1–1000 ppm in humidified hydrogen (97% H_2, 3% H_2O to 10% H_2, 90% H_2O). (d) Phase equilibrium of the Ni–O–S system at 1273 K. The shaded area shows the phases of Ni over an H_2S range of 1–1000 ppm in humidified hydrogen (97% H_2, 3% H_2O to 10% H_2, 90% H_2O).

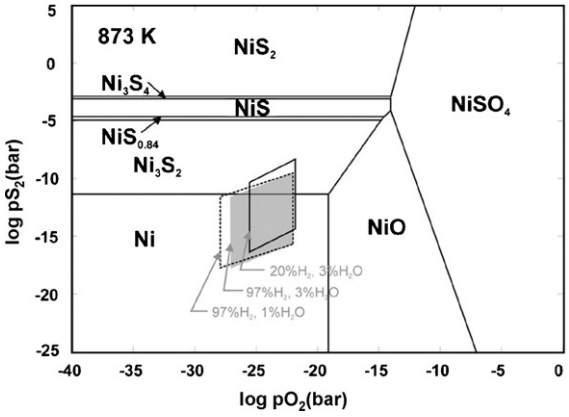

Fig. 2. Phase equilibrium of the Ni–O–S system at 873 K. The shaded area shows the phases of Ni in humidified hydrogen (97% H_2, 3% H_2O to 10% H_2, 90% H_2O; i.e. 90% fuel utilisation). The area defined by the solid lines shows the phases of Ni with an input of 20% H_2 and 3% H_2O balance N_2 (90% fuel consumption, H_2S range of 1–1000 ppm). The area defined by the dotted lines shows the phases of Ni with an input of 97% H_2 and 1% H_2O balance Ni (90% fuel consumption, H_2S range of 1–1000 ppm).

of H_2 at the input to the fuel cell can also be thought to represent the fuel mixture found in coal syngas [20]. With 90% fuel consumption, a fuel mixture of 20% H_2 and 3% H_2O, balance N_2, provides the output of 2% H_2 and 21% H_2O, balance N_2. This represents the solid-line bounds at 873 K shown in Figs. 2 and 5.

To study the impact of pH_2O on the propensity of sulphur to interact with Ni and ceria, a low amount of H_2O in the gas input was chosen as a fuel mixture of 1% H_2O and 97% H_2, balance N_2. With 90% fuel consumption, a fuel mixture of 97% H_2 and 1% H_2O, balance N_2, gives and output composition of 10% H_2 and 88% H_2O, balance N_2. The bounds at 873 K, presented as the dotted lines, are shown in Figs. 2 and 5. The values of pO_2 and pS_2 at the bounds for different fuel mixture inputs are shown in Table 2.

3. Thermodynamic predictions

The phases of Ni and ceria in the H_2S range of 1–1000 ppm in humidified fuels over the composition range equivalent to 3% H_2O, 97% H_2 to 90% H_2O, 10% H_2 are defined by the shaded area in each of the diagrams shown in Figs. 1–5.

Table 1
The values of pO_2 and pS_2 for different operating conditions in a range of H_2S from 1–1000 ppm (a fuel mixture of 97% H_2 and 3% H_2O was used as the input, with 90% fuel consumption—providing 10% H_2 and 90% H_2O as the output)

Temperature (K)	Bounds at the input (97% H_2, 3% H_2O)			Bounds at the output (10% H_2, 90% H_2O)		
	pO_2	pO_2, 1 ppm	pO_2, 1000 ppm	pO_2	pS_2, 1 ppm	pS_2, 1000 ppm
673	2.21×10^{-36}	1.62×10^{-21}	1.62×10^{-15}	2.00×10^{-31}	1.62×10^{-19}	1.62×10^{-13}
873	1.23×10^{-27}	2.33×10^{-18}	2.33×10^{-12}	1.12×10^{-22}	2.33×10^{-16}	2.33×10^{-10}
1073	4.08×10^{-22}	2.34×10^{-16}	2.34×10^{-10}	3.69×10^{-17}	2.34×10^{-14}	2.34×10^{-8}
1273	2.60×10^{-18}	5.61×10^{-15}	5.61×10^{-9}	2.35×10^{-13}	5.61×10^{-13}	5.61×10^{-7}

Table 2
The values of pO_2 and pS_2 in a range of H_2S from 1 ppm to 1000 ppm at 873 K for different input of fuel mixtures

Input	Bounds at the input			Bounds at the output		
	pO_2	pS_2, 1 ppm	pS_2, 1000 ppm	pO_2	pS_2, 1 ppm	pS_2, 1000 ppm
20% H_2, 3% H_2O	2.90×10^{-26}	5.48×10^{-17}	5.48×10^{-11}	1.42×10^{-22}	5.48×10^{-15}	5.48×10^{-9}
97% H_2, 1% H_2O	1.37×10^{-28}	2.33×10^{-18}	2.33×10^{-12}	1.07×10^{-22}	2.33×10^{-16}	2.33×10^{-10}

The Gibbs free energy of formation (ΔG_f) values of the compounds used to generate the Ni–O–S and the Ce–O–S system at 873 K and the corresponding references are presented in Tables 3 and 4, respectively. The tables also present the equations used to establish the temperature dependence of the ΔG_f values, covering the temperatures of the phase diagrams in this study.

3.1. Nickel phase behaviour

As shown in Fig. 1(a)–(d), eight possible compounds of nickel with sulphur and oxygen; Ni, Ni_3S_2, $NiS_{0.84}$, NiS, Ni_3S_4, NiS_2, $NiSO_4$ and NiO, can form depending on the reactant conditions. It can be seen in Fig. 1(a) and (b) that at 673 K and 873 K the operating boundary straddles the two phases of Ni and Ni_3S_2 depending on the concentration of H_2S. Ni_3S_2 is the dominant phase at 673 K, and Ni at 873 K. At 1073 K the operating boundary is mostly in the Ni phase as shown in Fig. 1(c); and almost completely in the Ni phase at 1273 K as shown in Fig. 1(d). This shows that as temperature decreases, the propensity of Ni to react with sulphur tends to increase, although decreasing temperature actually lowers the pS_2 level. At an operating temperature of 873 K, Ni_3S_2 forms only at H_2S concentrations higher than approximately 140 ppm, corresponding to other work [32] which reported that nickel exists in the metallic state only at pH_2S/pH_2 values below 10^{-3} to 10^{-4}. As shown in Fig. 1(b), sulphur interaction is favourable at H_2S concentrations above 140 ppm at the output composition while it is unfavourable at the input composition.

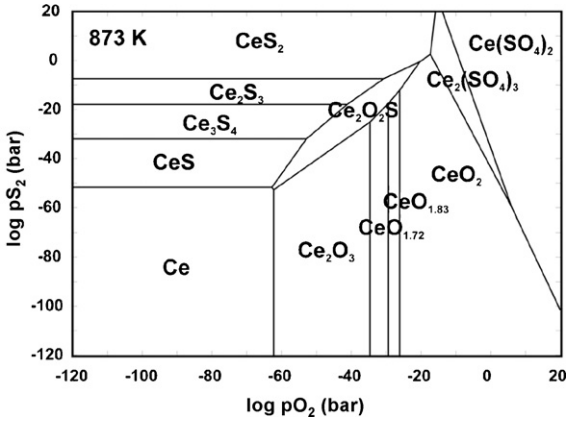

Fig. 3. Phase equilibrium of the Ce–O–S system at 873 K across a pO_2 and pS_2 range of 10^{-120} to 10^{20} bar.

It is of interest to study the effect of pH_2 and pO_2 on the reaction of Ni with sulphur in more detail by isolating the effect of one from the other. When the reaction of Ni with sulphur at the input and output compositions are considered, it can be seen that at the output, where the pH_2 is less than that at the input, the reaction of Ni with sulphur occurs at a lower H_2S concentration, as shown in Fig. 1(b). Fig. 2 shows the comparison between the phases of Ni for input mixtures of 97% H_2 and 20% H_2 (both with 3% H_2O, balance N_2) in order to see the effect of change in pH_2 with constant pO_2. The phases with an input composition of 97% H_2 and 3% H_2O (90% fuel consumption, H_2S range of 1–1000 ppm) are shown in the shaded area, while those with an input composition of 20% H_2 and 3% H_2O balance N_2 (90% fuel consumption, H_2S range of 1–1000 ppm) are defined by the solid lines. It can be seen that the decrease in pH_2 raises the pS_2 level—such that the reaction of sulphur with Ni occurs at lower H_2S concentrations. As shown in Fig. 2, the area defined by the dotted lines shows the phase of Ni with an input composition of 97% H_2 and a lower steam content of 1% H_2O, balance N_2 (90% fuel consumption, H_2S range of 1–1000 ppm) in order to see the effect of a change in pO_2 with constant pH_2. It can be seen that the change in humidity content, which in turn influences the pO_2, does not have a significant impact on the pS_2 level, and therefore does not significantly increase the extent of the reaction of sulphur with Ni.

The eight phases predicted to be present in the Ni–O–S system agree with previous work by Shariat and Behgozin [32], which is based on the reference of Knacke et al. [27], though a broader set of reference data was used in this study [21–31]. Among the eight compounds, $NiS_{0.84}$, NiS and Ni_3S_4 are not

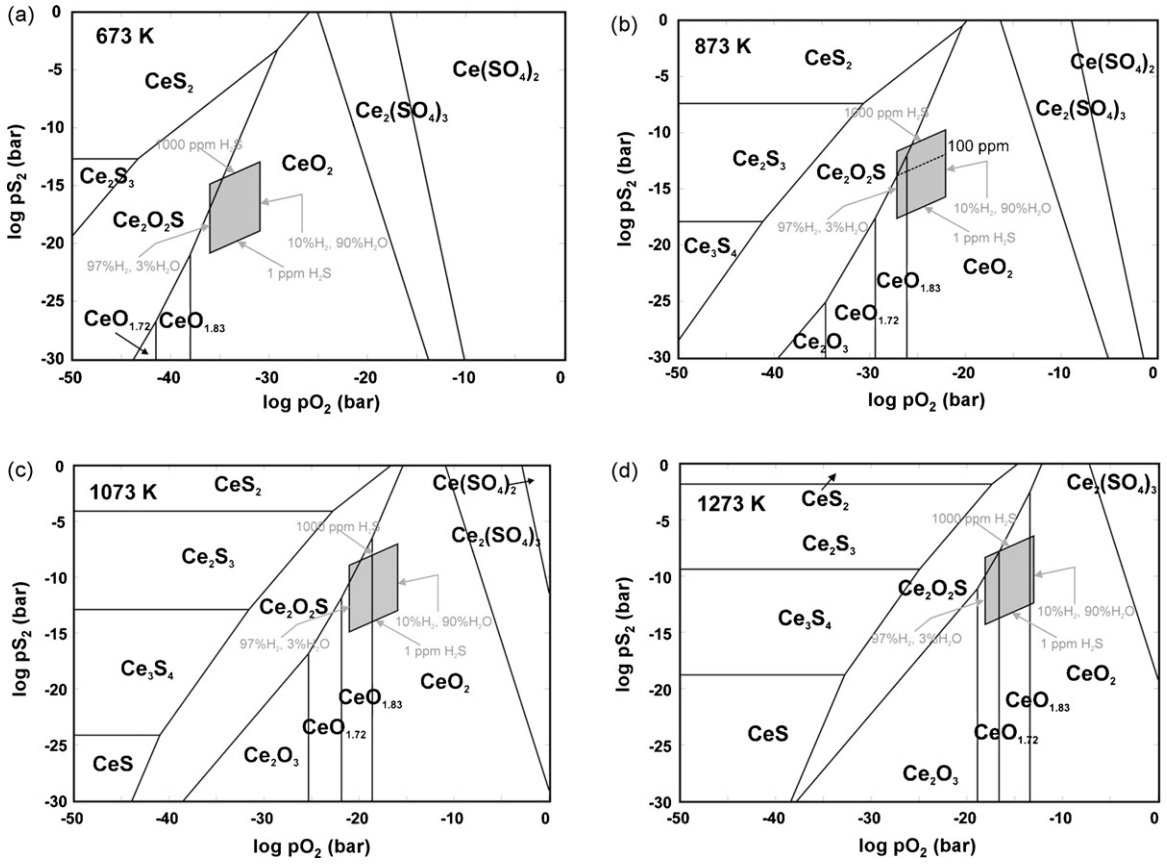

Fig. 4. (a) Phase equilibrium of the Ce–O–S system at 673 K. The shaded area shows the phases of ceria over an H_2S range of 1–1000 ppm in humidified hydrogen (97% H_2, 3% H_2O to 10% H_2, 90% H_2O). (b) Phase equilibrium of the Ce–O–S system at 873 K. The shaded area shows the phases of ceria over an H_2S range of 1–1000 ppm in humidified hydrogen (97% H_2, 3% H_2O to 10% H_2, 90% H_2O). The dotted line in the shaded area shows an H_2S concentration of 100 ppm. (c) Phase equilibrium of the Ce–O–S system at 1073 K. The shaded area shows the phases of ceria over an H_2S range of 1–1000 ppm in humidified hydrogen (97% H_2, 3% H_2O to 10% H_2, 90% H_2O). (d) Phase equilibrium of the Ce–O–S system at 1273 K. The shaded area shows the phases of ceria over an H_2S range of 1–1000 ppm in humidified hydrogen (97% H_2, 3% H_2O to 10% H_2, 90% H_2O).

stable at all temperatures. $NiS_{0.84}$ is stable at 673 and 873 K, while NiS is stable at 873 K and 1073 K. At temperature above 845 K Ni_3S_2 can change to Ni_3S_4 [33]. This may result in Ni_3S_4 being present in the phase diagrams at 873 K, 1073 K and 1273 K. However, it should be noted that the main phases in the Ni–O–S system across the bounds of fuel cell operation in this study are Ni and Ni_3S_2, which are stable across the temperature and pS_2/pO_2 range studied.

Table 3
ΔG_f values of compounds used to generate the Ni–O–S diagram at 873 K

Compound	ΔG_f (kJ/mol) at 873 K	Temperature dependence	Reference
Ni	−36.8	$-0.051T + 11.4$ for 631 K $\leq T <$ 700 K	[21]
		$-0.065T + 19.7$ for 700 K $\leq T <$ 1200 K	[21]
		$-0.08T + 37.6$ for 1200 K $\leq T <$ 1728 K	[21]
Ni_3S_2	−383.5	$-0.21T - 187.0$ for 298 K $\leq T <$ 829 K	[22,23]
		$-0.36T - 66.6$ for 829 K $\leq T <$ 1062 K	[22]
		$-0.56T + 197.7$ for 1062 K $\leq T <$ 3800 K	[22,24,25]
$NiS_{0.84}$	−142.2	$-0.078T - 71.8$ for 298 K $\leq T <$ 833 K	[26]
NiS	−155.0	$-0.12T - 47.5$ for 652 K $\leq T <$ 1249 K	[22]
		$-0.21T - 76.1$ for 1249 K $\leq T <$ 3400 K	[27,24,25]
Ni_3S_4	−532.2	$-0.35T - 234.7$ for 298 K $\leq T <$ 1100 K	[27,24,25]
NiS_2	−221.1	$-0.14T - 101.8$ for 298 K $\leq T <$ 1280 K	[22]
$NiSO_4$	−1004.5	$-0.21T - 825.6$ for 298 K $\leq T <$ 1200 K	[22,25]
NiO	−291.6	$-0.08T - 220.1$ for 600 K $\leq T <$ 750 K	[25]
		$-0.12T - 180.5$ for 750 K $\leq T <$ 2230 K	[25]

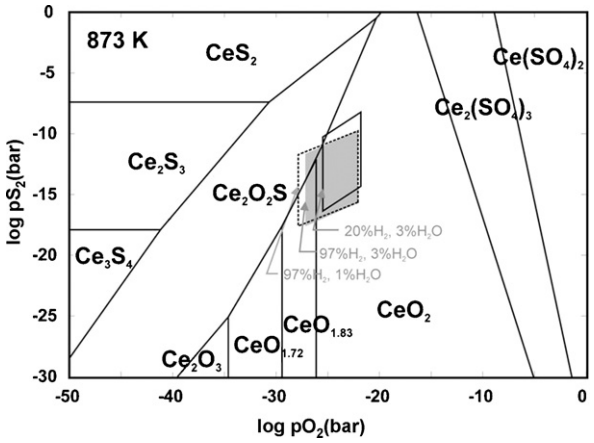

Fig. 5. Phase equilibrium of the Ce–O–S system at 873 K. The shaded area shows the phases of ceria with an input of 97% H_2 and 3% H_2O (90% fuel consumption, H_2S range of 1–1000 ppm). The area defined by the solid lines shows the phases of ceria with an input of 20% H_2 and 3% H_2O balance N_2 (90% fuel consumption, H_2S range of 1–1000 ppm). The area defined by the dotted lines shows the phases of ceria with an input of 97% H_2 and 1% H_2O balance N_2 (90% fuel consumption, H_2S range of 1–1000 ppm).

3.2. Ceria phase behaviour

Fig. 3 shows the equilibrium system of ceria with sulphur and oxygen at 873 K across the pO_2 and pS_2 range from 10^{-120} to 10^{20}. Twelve phases: Ce, CeS, Ce_3S_4, Ce_2S_3, CeS_2, Ce_2O_2S, Ce_2O_3, $CeO_{1.72}$, $CeO_{1.83}$, CeO_2, $Ce_2(SO_4)_3$ and $Ce(SO_4)_2$ are predicted in the Ce–O–S system. It can be seen in Fig. 4(a) that at 673 K the Ce–O–S system is resident in the CeO_2 and Ce_2O_2S forms. At 873 K, as shown in Fig. 4(b), CeO_2 can be reduced to $CeO_{1.83}$ depending on the pO_2. Thus, there is a mixture of CeO_2, $CeO_{1.83}$, and Ce_2O_2S at 873 K. At 1073 K, the operating boundary covers a larger area of the $CeO_{1.83}$ phase and also spans the phases of CeO_2 and Ce_2O_2S (Fig. 4(c)). At 1273 K, $CeO_{1.83}$ is the dominant phase and the system also extends into the phase of $CeO_{1.72}$—indicating that a mixture of CeO_2, $CeO_{1.83}$, $CeO_{1.72}$ and Ce_2O_2S can be present as shown in Fig. 4(d). Fig. 4 illustrates that the reduction to non-stoichiometric ceria is more favourable as pO_2 decreases and temperature increases, in agreement with experimental work [10–12].

Fig. 4(b) shows the phase diagram at 873 K, with certain concentrations of H_2S explicitly stated. It can be seen that an H_2S concentration around 100 ppm is likely to be the maximum level at which the CeO_2 is stable, avoiding the irreversible incorporation of sulphur at the input composition.

The pO_2 has a significant impact on the interaction of sulphur with ceria at 873 K as shown in Fig. 5. The shaded area shows the phases of ceria when exposed to sulphur with an input composition of 97% H_2 and 3% H_2O (90% fuel consumption, H_2S range of 1–1000 ppm) while the area defined by the dotted lines shows the bounds when the humidity content in the input composition was lowered to 1%. The area defined by the solid lines shows the phases of ceria exposed to sulphur when the H_2 content was changed to 20%. As shown in Fig. 5, the decrease in pO_2 causes the domain to cover a greater area of the Ce_2O_2S phase—suggesting that the reaction of sulphur with ceria becomes more favourable as pO_2 decreases.

In this calculation, variations of pO_2 were investigated that simulate the range of values expected to be found across the flow-field of an SOFC operating at 90% fuel consumption, with a hydrogen feed. At 873 K, the pO_2 lies in the range from 10^{-27} to 10^{-22} across the input to output composition. At the input fuel composition ceria can form stable $CeO_{1.83}$ such that the reaction of $CeO_{1.83}$ with sulphur tends to be more favourable than that of Ni (at the input composition the reaction of $CeO_{1.83}$ with sulphur occurs at H_2S concentrations above 100 ppm while that of Ni is unfavourable). However, ceria tends to be more stable than Ni at higher pO_2 (approx. $>10^{-26}$) where ceria exists as the CeO_2 phase.

Among the twelve stable phases existing in the diagrams, Ce_2O_2S is the most influential phase in determining the reaction of sulphur with ceria under the operating condition of an SOFC. Therefore, the phase boundary between CeO_{2-x} and Ce_2O_2S is very important in predicting the impact of sulphur on ceria, and the accuracy of the boundary critically relies on the reference data of the compound. Eqs. (8)–(10) compare the ΔG_f for the formation of Ce_2O_2S as a function of temperature reported by

Table 4
ΔG_f values of compounds used to generate the Ce–O–S diagram at 873 K

Compound	ΔG_f (kJ/mol) at 873 K	Temperature dependence	Reference
		$-0.099T + 14.7$ for 600 K $\leq T <$ 999 K	[22]
Ce	−71.2	$-0.11T + 26.8$ for 999 K $\leq T <$ 1071 K	[22]
		$-0.15T + 75.7$ for 1071 K $\leq T <$ 3695 K	[22]
CeS	−544.8	$-0.15T - 418.3$ for 298 K $\leq T <$ 1900 K	[28,26,25]
Ce_3S_4	−1943.0	$-0.42T - 1581.7$ for 298 K $\leq T <$ 1200 K	[26]
Ce_2S_3	−1359.1	$-0.35T - 1064.6$ for 298 K $\leq T <$ 2000 K	[28]
CeS_2	−731.2	$-0.16T - 593.4$ for 298 K $\leq T <$ 1152 K	[27]
Ce_2O_2S	−1855.4	$-0.28T - 1624.4$ for 298 K $\leq T <$ 1700 K	[27]
Ce_2O_3	−1988.7	$-0.28T - 1757.3$ for 298 K $\leq T <$ 1300 K	[29,25,30]
$CeO_{1.72}$	−1078.9	$-0.13T - 971.1$ for 298 K $\leq T <$ 1200 K	[26]
$CeO_{1.83}$	−1116.5	$-0.13T - 1010.5$ for 298 K $\leq T <$ 1200 K	[26]
CeO_2	−1169.7	$-0.18T - 1022.0$ for 298 K $\leq T <$ 2753 K	[22,29,25]
$Ce_2(SO_4)_3$	−4318.6	$-0.52T - 3864.1$ for 298 K $\leq T <$ 1000 K	[26]
$Ce(SO_4)_2$	−2519.1	$-0.20T - 2343.0$ for 298 K $\leq T <$ 398 K	[31]

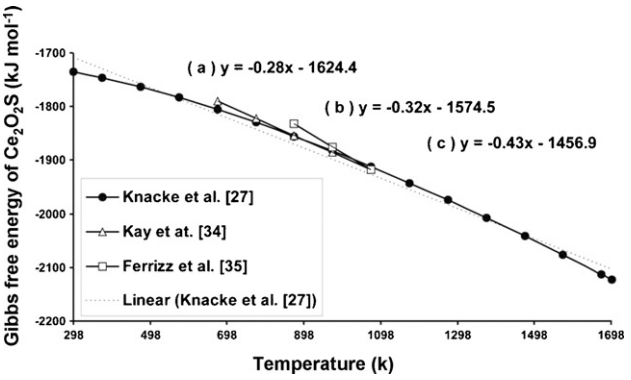

Fig. 6. Comparison of Gibbs free energy of Ce_2O_2S formation using different sources of reference data (a) [27] (b) [34], (c) [35].

Knacke et al. [27] (used in this study), Kay et al. [34], and Ferrizz et al. [35], respectively.

$$\Delta G_f = -0.28T - 1624.4 \quad \text{for } 298\,K < T < 1700\,K \tag{8}$$

$$\Delta G_f = -0.32T - 1574.5 \quad \text{for } 673\,K < T < 1073\,K \tag{9}$$

$$\Delta G_f = -0.43T - 1456.9 \quad \text{for } 873\,K < T < 1073\,K \tag{10}$$

As shown in Fig. 6, the ΔG_f values used in this study (Knacke et al. [27]) are in good agreement with those of Kay et al. [34]. The ΔG_f values of Ferrizz et al. [35] are however, higher between 873 K and 1000 K, which would alter the predicted boundary of sulphide formation, increasing its onset from a H_2S concentration of 100 ppm, which is derived from this study, to approximately 2600 ppm when considered at 873 K and a pO_2 of 10^{-27}. The phase diagrams reported by Kay et al. were derived from reference [36] whereas the results from Ferrizz et al. were constructed using data derived experimentally from temperature programmed oxidation. The data of Ferrizz et al. is consistent with that of Key et al. at 1073 K. As temperature decreases to 973 K and 873 K, a larger deviation from the results of Kay et al. was reported by the Ferrizz study; this deviation corresponding to a difference in the predicted limit of sulphur tolerance of Ni to S of one and three order of magnitude, respectively. The disparity between the results in the literature suggests that further experimental work is necessary to better define the phase boundary.

The thermodynamic data predicted in this study represent the behaviour of the bulk phases under equilibrium conditions. The thermodynamic predictions show that Ni and ceria are stable when exposed to 100 ppm H_2S at 873 K, suggesting that sulphur at this level will not affect the bulk properties of a Ni-CGO anode. Although the calculation shows that bulk sulphide formation of Ni and ceria is not likely under these conditions, the reaction of sulphur on surface needs to be considered. Future work is focused on understanding the impact of sulphur on the surface behaviour, and in turn on the catalytic properties, of Ni and ceria.

4. Conclusion

Using thermodynamics calculations, the effect of pO_2 and pS_2 on the phase behaviour of Ni and ceria has been studied over a range of values which cover the bounds of practical IT-SOFC operation on sulphur-containing fuels. The reaction of Ni with sulphur is predicted to become more favourable as temperature and hydrogen partial pressure (pH_2) decrease. Ceria is shown to become increasingly non-stoichiometric (CeO_n, $n < 2$) as pO_2 decreases and temperature increases, and it is predicted that its reaction with sulphur becomes more favourable under these conditions. It is clear from this study that Ni and ceria do not form any bulk sulphide phases at up to 100 ppm H_2S. The impact of sulphur on the surface properties of the anode is now under consideration.

An interesting consequence of this analysis is that the reaction of sulphur with ceria is more likely to occur at the start of a flow-field, where the pO_2 of the fuel stream is lowest. It may therefore be possible use pO_2 to control the impact of sulphur in this regime.

References

[1] W. Vielstich, A. Hubert, Handbook of Fuel Cells-Fundamentals, Technology and Applications, John Wiley & Sons, New York, 2003.
[2] http://www/hydro.com (last access: 25 September 2006).
[3] http://www.petrochem-ir.net (last access: 25 September 2006).
[4] X. Ma, L. Sun, C. Song, Catal. Today 77 (2002) 107–116.
[5] P.J. de Wild, R.G. Nyqvist, F.A. de Bruijn, E.R. Stobbe, J. Power Sources 159 (2006) 995–1004.
[6] C.H. Bartholomew, P.K. Agrawal, Sulphur Poisoning on Metals, Academic Press, 1982.
[7] L.L. Hegedus, R.W. McCabe, Catalyst Poisoning, Marcel Dekker, New York, 1984.
[8] J. Dong, Z. Cheng, S. Zha, M. Liu, J. Power Sources 156 461–465.
[9] V.B. Tare, J.B. Wagner Jr., J. Appl. Phys. 54 (1983) 252–257.
[10] B.H.C. Steele, Solid State Ionics 129 (2000) 95–110.
[11] A. Trovarelli, C.D. Leitenburg, M. Boaro, G. Dolcetti, Catal. Today 50 (1999) 353–367.
[12] Y. Zeng, S. Kaytakoglu, D.P. Harrison, Chem. Eng. Sci. 55 (2000) 4893–4900.
[13] Y. Zeng, S. Zhang, F.R. Groves, D.P. Harrison, Chem. Eng. Sci. 154 (1999) 3007–3017.
[14] E. Aneggi, M. Boaro, C. de Leitenburg, G. Dolcetti, A. Trovarelli, J. Alloy Compd. 408–412 1096–1102.
[15] S. Wang, T. Kobayashi, M. Dokiya, T. Hashimoto, J. Electrochem. Soc. 147 (2000) 2606–3609.
[16] H.J. Park, G.M. Choi, J. Eur. Ceram. Soc. 24 (2004) 1313–1317.
[17] N.P. Brandon, D.J.L. Brett, Philos. Trans. R. Soc. A 364 (2006) 147–159.
[18] P.K. Cheekatamarla, A.M. Lane, J. Power Sources 152 (2005) 256–263.
[19] OUTOKUMPU, HSC Chemistry for Windows, Version 5.1, OUTOKUMPU.
[20] A.I. Marquez, T.R. Ohrn, J.P. Trembly, D.C. Ingram, D.J. Bayless, J. Power Sources 164 (2007) 659–667.
[21] NASA, Thermodynamic data for fifty reference elements, NASA-TP-3287, N93-19977, 1993.
[22] I. Barin, Thermochemical Data of Pure Substances, VCH Verlags Gesellschaft, Weinheim, 1993.
[23] K.C. Mills, Thermodynamic Data for Inorganic Sulphides, Selenides and Tellurides, Butterworths, London, 1974.
[24] M.W. Chase Jr., C.A. Davies, J.R. Downey Jr., D.J. Frurip, R.A. McDonald, A.N. Syverud, J. Phys. Chem. Ref. Data 14 (1985) 927–1856.

[25] Scientific Group Thermodata Europe (SGTE), Thermodynamic Properties of Inorganic Material, Landolt-Börnstein, Springer-Verlag, Berlin, Heidelberg, 1999.
[26] I. Barin, O. Knacke, O. Kubaschewski, Thermodynamic Properties of Inorganic Substances, Springer-Verlag, New York, 1973, Supplement 1977.
[27] O. Knacke, O. Kubaschewski, K. Hasselman, Thermochemical Properties of Inorganic Substances, Springer-Verlag, Berlin, 1991.
[28] T.G.S. Kosolapovoi, Polysenie I Primenie Tugoplavkih Soedinenij, Moskva, 1986.
[29] Glushko Thermocenter of the Russian Academy of Sciences, IVTAN Association, Izhorskaya, Moscow, 1994.
[30] M.E. Huntelaar, A.S. Booij, E.H.P. Cordfunke, R.R. van der Laan, A.C.G. van der Genderen, J.C. van Miltenburg, J. Chem. Thermodyn. 32 (2000) 465–482.
[31] G. Fabricius, S. Liukkonen, G. Sundholm, Fysikaalisen Kemian Taulukoita, Otatieto, Espoo, 1994.
[32] M.H. Shariat, S.A. Behgozin, Calphad 20 (1996) 47–67.
[33] R.Y. Lin, D.C. Hu, Y.A. Change, Met. Trans. 9B (1978) 531–538.
[34] D.A.R. Kay, W.G. Wilson, V. Jaran, J. Alloy Compd. 192 (1993) 11–16.
[35] R.M. Ferrizz, R.J. Gorte, J.M. Vohs, Appl. Catal. 43 (2003) 273–280.
[36] R.K. Dwivedi, D.A.R. Kay, J. Less-Common Met. 102 (1984) 1–7.